Autism Spectrum Disorder Detection using Variable Frequency Complex Demodulation of the Electroretinogram

Hugo F. Posada-Quintero, Sultan Mohammad Manjur, Md. Billal Hossain, Fernando Marmolejo-Ramos, Irene O. Lee, David H. Skuse, Dorothy A. Thompson, Paul A. Constable

Keywords: Electroretinogram, Signal Analysis, Autism Spectrum Disorder, Machine Learning

Abstract:

The early diagnosis of neurodevelopmental conditions such as autism spectrum disorder (ASD), is an unmet need. One difficulty is the identification of a biological signal that relates to the ASD phenotype. The electroretinogram (ERG) waveform has been identified as a possible signal that could categorize neurological conditions such as ASD. The ERG waveform is derived from the electrical activity of photoreceptors and retinal neurons in response to a brief flash of light and provides an indirect 'window' into the central nervous system. Traditionally, the waveform is analyzed in the time-domain, but more recently time-frequency spectrum (TFS) analysis of ERG has been successfully carried out using discrete wavelet transformation (DWT) to characterize the morphological features of the signal. In this study, we propose the use of a high resolution TFS technique, namely variable frequency complex demodulation (VFCDM), to decompose the ERG waveform based on two signal flash strengths to build machine learning (ML) models to categorize ASD. ERG waveforms from N=217 subjects (71 ASD, 146 control), at two different flash strengths, 446 and 113 Troland seconds (Td.s), from both right and left eyes were included. We analyzed the raw ERG waveforms using DWT and VFCDM. We computed features from the TFSs and trained ML models such as Random Forest, Gradient Boosting, Support Vector Machine to classify ASD from controls. ML models were validated using a subject independent validation strategy, and we found that the ML models with VFCDM features outperformed models using the DWT, achieving an area under the receiver operating characteristics curve of 0.90 (accuracy = 0.81, sensitivity = 0.85, specificity = 0.78). We found that the higher frequency range (80 - 300 Hz) included more relevant information for classifying ASD compared to the lower frequencies. We also found that the stronger flash strength of 446 Td.s in the right eye provided the best classification result which supports VFCDM analysis of the ERG waveform as a potential tool to aid in the identification of the ASD phenotype.

1. Introduction

Autism Spectrum Disorder (ASD) is a neurodevelopmental condition characterized by difficulties in reciprocal social interactions, communication, and repetitive/restrictive behaviors [1], [2]. Early interventions and appropriate support can help individuals with ASD improve their quality of life [3]. Unfortunately, the large heterogeneity observed in the ASD phenotype may

result in a delayed diagnosis [4]. In this paper, our goal was to test and validate the feasibility of the electroretinogram (ERG) as a potential biomarker to facilitate the diagnosis of ASD. Biomarker discovery in ASD has shown some promise with eye movements gaining attention in this space as the most promising indicator of ASD in early childhood [5]–[8]. In addition, several other potential biological signals such as heart rate variability (HRV) [9], electrodermal activity (EDA) [10], and electroencephalogram (EEG) [11], [12] have also been used to help identify ASD at an early stage of development [4]. Despite promising results with these noninvasive signals, the recording of these biological signals can be cumbersome and may require specialist skills and knowledge which may hinder their wider application in clinical settings. For instance, collecting EEG signals require several electrodes and knowledge about the electrodes' positioning, making the development of tools for the general population based on EEG signals difficult [13]. EDA is a very sensitive neurophysiological marker, although it is highly affected by emotions and noise artifacts [14] which can limit its specificity. HRV is a widely used tool to assess the autonomic nervous system because it provides useful information, but sympathetic and parasympathetic control overlap in HRV, and stress and other external factors can affect HRV parameters [15]. Therefore, the identification of a biosignal that is independent of emotion and stress, and easily recorded is desirable to facilitate the development of a simple and practical tool for the early diagnosis of ASD by health care professionals.

The retina, as an extension of the central nervous system, is viewed as a 'window to the brain' [16]. Several commentaries and recent reviews have identified the potential use of the ERG waveform in the diagnosis and management of psychiatric disorders encompassing neurodevelopment and neurodegenerative conditions [17]–[19]. The main rationale for using the ERG signal is that the main neurotransmitters such as glutamate, GABA and dopamine contribute to the ERG waveform's shape and the regulation and/or signaling pathways of these neurotransmitters have been implicated in the pathophysiology of several psychiatric disorders [20]–[23]. As such the functional changes in the retina, as recorded with the ERG provides a readily accessible neural pathway that can be used to study a range of neurodevelopmental and neurodegenerative disorders, including ASD, schizophrenia, bipolar disorder, Parkinson's, and depression [24]. For instance, Constable et al., Lee et al., and Ritvo et al. have found a reduced peak b-wave amplitude in children with ASD compared to controls with typical development under dark and light adapted conditions [25]–[27]. However, these findings may not extend to an adult population of ASD individuals when limited to time-domain parameters [28].

Traditional analyses of the ERG waveform have focused on time-domain parameters, such as the amplitudes and time to peaks of the two principal waveform components known as the a- and b-wave [28]–[32]. Recent findings in the b-wave amplitude of the ERG suggest it may be possible to differentiate ASD and other neurodevelopmental disorders such as attention deficit hyperactivity disorder (ADHD) using time-domain indices extracted from the ERG signal [25].

Despite being limited to time-domain indices, these studies provide evidence that a more in-depth analysis in the spectral-domain could aid our understanding of these neurological conditions through an understanding of the neural pathways and neurotransmitters involved in contributing to the components of the overall ERG waveform [32].

In TFS analysis of the ERG waveform, DWT has provided accurate identification of the morphological features of the signal [32], [33]. For instance, Gauvin et al. used the Haar wavelet to perform a DWT analysis on the ERG waveform and characterized the frequency content of different morphological features of the ERG waveform [32], [34], [35]. Their findings identified key central frequencies associated with the ON and OFF retinal pathways in the 'a' and 'b' waves (20 and 40Hz), as well as the early and later oscillatory potentials (OPs) at 80 and 160 Hz, respectively [35].. Despite promising results, there has not been any research to validate and further extend the possibilities of ERG as a potential biomarker in ASD. Additional TFS analyses of the ERG may provide alternative sensitive features beyond the time-domain indices that could help to identify the phenotype of different neurodevelopmental disorders such as ASD. Our preliminary results suggest that the extracted features can be used for training ML models for ASD detection [36]. To extend these findings we have implemented a high-resolution spectral decomposition technique, namely variable frequency complex demodulation (VFCDM), that has been used previously for the TFS analysis of biomedical signals [37], [38] and evaluated the sensitivity of the extracted features for ASD detection using ML models, compared to DWT and time-domain features.

Therefore, we hypothesize that the ERG waveforms analyzed with TFS techniques could enable a more accurate and reliable basis with which to detect ASD, compared to conventional time-domain measures. In this study, we analyzed the ERG waveforms in the time and TFS domains and applied well established ML techniques such as Random Forest (RF) [39], Gradient Boosting (GradBoost) [40], Adaptive Boosting (AdaBoost) [41], Extreme Gradient Boosting (XGBoost) [42], Support Vector Machine (SVM) [43], K nearest neighbor (KNN) [44], Multilayer Perceptron (MLP) [45] to identify the ASD phenotype. Specifically, we found that VFCDM, with a high resolution spectral decomposition [38], was most effective at developing a classification model for ASD, compared to other methods, based on the light-adapted ERG waveforms examined.

2. Related Works

In clinical settings, the Autism Diagnostic Observation Schedule [46] and the Autism Diagnostic Interview [47] are considered the gold standards for assessing ASD [48]. Other observational ASD assessment procedures are the Child Autism Rating Scale [49], the Social Communication Questionnaire [50], the Social Responsiveness Scale [51] and the Developmental, Dimensional and Diagnostic Interview (3Di) [52]. However, these traditional ASD assessment

procedures are time consuming and can be influenced by the interpretation and expertise of the examiner. Therefore, the identification of an additional biomarker of ASD may help improve the diagnostic accuracy and reduce the overall test duration required to form a diagnosis in some cases [53].

Several possible biosignals have been explored in the last decades to establish a potential and reliable biomarker that can provide an objective clinical marker for the ASD phenotype that is supported by clinical diagnostic tests such as the ADOS and ADI. For instance, leveraging on the fact that ASD individuals exhibit atypical visual scan paths during social interactions [8], eye movements has beenone of the most explored signals to develop biomarkers for ASD detection [48]. Carette et al. proposed an LSTM-based ML model using features computed from eye movement data to classify ASD from typical individuals and achieved a classification accuracy of 83% [54]. Kang et al. proposed a support vector machine learning model using features calculated from EEG and eye tracking data and were able to achieve an AUC score of 0.86 [55]. Along with atypical eye movements, ASD individuals tend to show reduced power in the alpha frequency band [56] of EEG signals and comparatively higher white matter in different brain regions [57]. In addition, Shoeibi et al. have proposed a CNN-LSTM-based ML model using EEG signals to predict schizophrenia with an accuracy of 99.25% [58]. Ari et al. have also reported high detection accuracy (98.88%) of ASD using pre-trained CNN models [59]. EDA [60], which provides an assessment of the sympathetic branch of the autonomic nervous system [61], has also been used to classify ASD based on different patterns during arousal and anxiety in toddlers with ASD compared to a typically developing comparison group [62], [63].

Another biosignal that has gained interest in recent years to study neurodegenerative and neurodevelopmental disorders such as schizophrenia, bipolar disorder, Alzheimer's and Parkinson's disease is the ERG [25], [30], [64]–[67] with several studies also reporting a reduced ERG b-wave amplitude in ASD individuals under light- and dark-adapted conditions for children and adults [25]–[27], [33], [65], [69]. Though several studies have reported promising observations using the ERG to investigate different disorders, and demonstrate its potential as a biomarker, none of these studies to date have harnessed the potential of ML algorithms with different signal analytical techniques with which to evaluate classification models.

3. Methods

For testing the feasibility of VFCDM processing of the ERG waveform signals to provide an accurate classification of ASD, we used a subset of previously collected ERG recordings from ASD and typical developing comparison (control) individuals from both eyes, at two flash strengths. Then, we processed the data using traditional time-domain methods, DWT, and VFCDM and extracted features to train ML models for ASD vs. control classification. The participants,

protocol, signal processing and analyzing methods, and ML classification are explained in this section.

3.1. Participants

A total of 217 individuals, 71 ASD, and 146 controls took part in previous studies that were recruited at two sites in London and Adelaide [25], [37], [68]. The median ages (range, ± std. deviation) of participants were ASD 14.5 (5.0-16.3, ±5.4) and control 12.4 (5.0-26.7, ±5.9) years (p=.008, Mann-Whiney U test). The difference in age between groups is not considered to have an effect on the ERG amplitudes in this young cohort with clear optical media [70]. There were 46 (65%) males in the ASD and 53 (37%) in the control group ($\chi^2(1)$, 17.2 p<.001. All ASD participants met diagnostic classification (DSM-IV-TR [71] or DSM-V [72]) based on assessments with either the ADOS (Autism Diagnostic Observation Schedule) [73], ADOS-2 [74] or 3Di) [52] performed by a pediatric psychiatrist or clinical psychologist in the social communication disorder clinics at Great Ormond Street Hospital for Children in the UK or local Child and Adolescent Mental Health clinics in South Australia. Control participants were recruited from advertisements on social media platforms and through word of mouth. The control participants had no family history of ASD or psychiatric illness. From either the ASD or control group, participants were excluded if there was a history of strabismus surgery or inherited retinal disease, chromosomal disorders such as Down's syndrome, diabetes, or co-occurrence of another neurodevelopmental disorder such as ADHD or a history of traumatic brain injury.

3.2. Electroretinogram Recording

The ERG recording protocol using the RETeval (LKC Technologies Inc, Gaithersburg, MD, USA) has been described in detail previously [25], [66], [68] and followed the International Society for Clinical Electrophysiology of Vision guidelines [75]. The sampling frequency of the collected ERG signals was 2000Hz. Based on the results of our previous studies [36], [25] that demonstrated strong group differences, we selected two flash strengths, 113 Td.s, and 446 Td.s, on a 1130 Td white background to examine in this study. With an assumed 6 mm pupil diameter, the equivalent white flash strengths were 0.60 and 1.20 log photopic cd.s.m^{-2} on a 40 cd.m^{-2} white background. Only waveforms with an a-wave amplitude < -1 μV were included [68].

The ERG was recorded from the right eye then left eye. Flashes were presented at a stimulus frequency of 2Hz at two flash strengths (113 or 446 Td.s). ERG Waveforms were averaged (30-60) to generate the reported averaged waveform which was used for further analysis. (It was not possible based on the RETeval firmware ver 2.12.0 at the time to randomize the 'eye' or to perform the test on the left eye first then the right eye). Traces were rejected from the average if they fell above or below the 25th centile. Replicates of the recordings were made in each eye

as required. All recordings were made under normal room lighting of 250-350 lux in undilated pupils. The raw waveform data, iris color, and images of the electrode position below the eye were exported using the RFF extractor version 2.9.4.1 (LKC Technologies Inc, Gaithersburg, MD, USA) [76]. The electrode position was measured using a scaled graticule with electrodes placed 2mm below the lower lid according to the manufacturer's recommendation given a reference value of 0, with electrodes higher a value of +1 and lower either -1 or -2 with traces excluded if the electrode was positioned > 2mm below the recommended height. The reader is directed to the original studies for further details [25], [33], [68].

Ethics and data origin

The original studies [25], [33], [68] from which data were analyzed in this paper were approved by the Flinders University Human Research Ethics Committee and the Southeast Scotland Research Ethics Committee in the United Kingdom and conformed to the tenets of the declaration of Helsinki. Written informed consent to participate in this study for those under 16 years of age was provided by the participants' legal guardian/next of kin with permission to re-use any data for future studies.

3.3. ERG waveform processing

Traditional analysis of ERG signals is based on time-domain measures of the time to peak and amplitudes of the main peaks and troughs of the ERG waveform. However, TFS analyses have been implemented process ERG signal further. For this study, we implemented both strategies for the ERG waveform signal processing, with the detailed methods described in this section. A general Framework of proposed method is provided in figure 1.

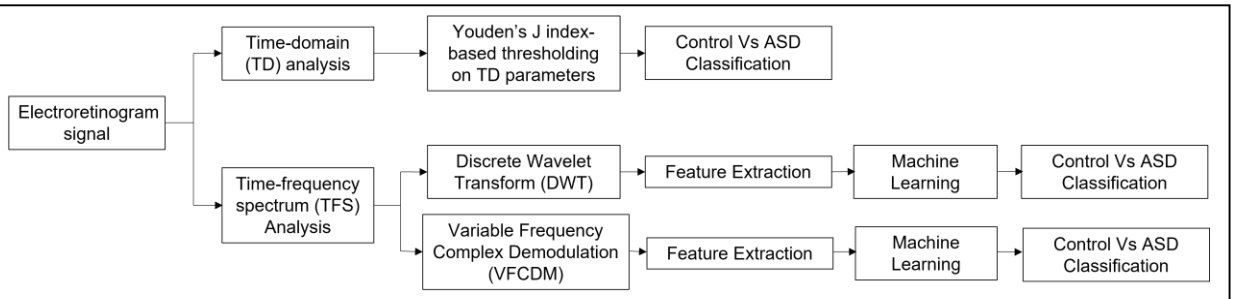

Figure 1: General Framework of the proposed approach.

3.3.1. Time-Domain indices of ERG

The light-adapted full-field ERG waveform provides is the recorded electrical response of the retina to a flash of light providing a quantitative measure of retinal function [25]. Figure 2

depicts an ERG waveform 'signal', where the first negative trough is termed the a-wave and mainly reflects the hyperpolarization of the cone photoreceptors in the light adapted ERG [77]. The subsequent b-wave is the result of second order bipolar cells in the ON- and OFF- pathways which may be shaped by additional potassium currents in glial cells [25], [78]. There are some low amplitude with high frequency oscillations in the ascending limb of the b-wave known as the oscillatory potentials (OPs) that are initiated by the amacrine cells [68].

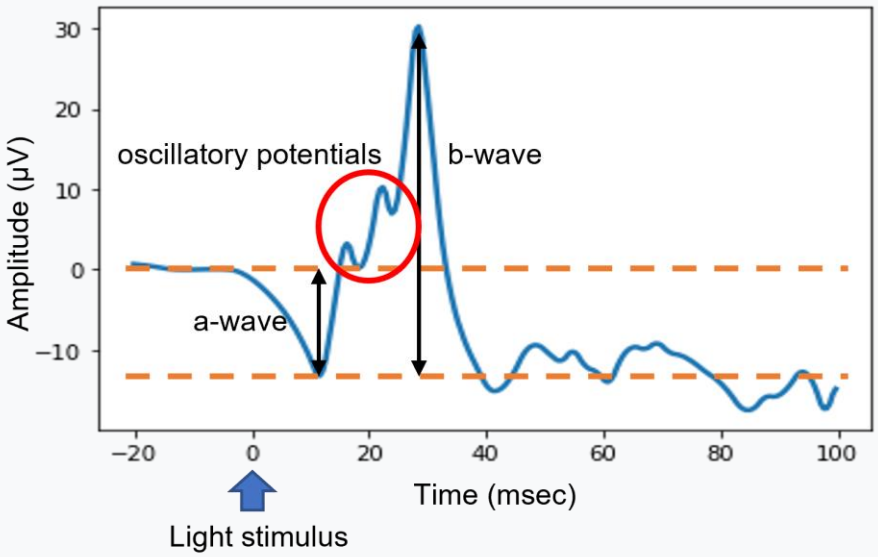

Figure 2: Electroretinogram signal with time-domain indices indicated by T_a (time from stimulus onset to the a-wave minima). V_a (amplitude of the a-wave measured from baseline to the minima). T_b (time from stimulus onset to b-wave maxima). V_b (b-wave amplitude measured from the minimum to maximum of the ERG signal. Note the Oscillatory Potentials (OPs) appear as small ripples on the ascending limb of the b-wave.

In this study, the a-wave and b-wave time to peak and amplitude were extracted from the raw waveforms using the RFF extractor software that localized the minima and maxima of the a- and b-waves and were confirmed by visual inspection for each included waveform to ensure correct identification [25], [33], [68]. Here, T_a and T_b are the time to peak of the a-wave and b-wave and V_a and V_b represent the amplitudes of the a- and b-wave respectively as defined in the ISCEV standard [75].

3.3.2. Discrete Wavelet Transform Analysis

The DWT can be expressed as a convolution between the raw signal $x(t)$ and the mother wavelet φ (t). $C\,(p, q)$ refers to the DWT coefficients in equation (1) where p and q are scaling and translational factors (with base equal to 2) respectively.

$$C(p,q) = \frac{1}{\sqrt{|p|}} \int_{-\infty}^{\infty} x(t) * \varphi\left(\frac{t-q}{p}\right) dt \quad (1)$$

Gauvin et al.[34], [35] has proposed a seven level decomposition of the ERG waveform signal and characterized different DWT descriptors using the TFS as shown in figure 3. The a-wave and b-

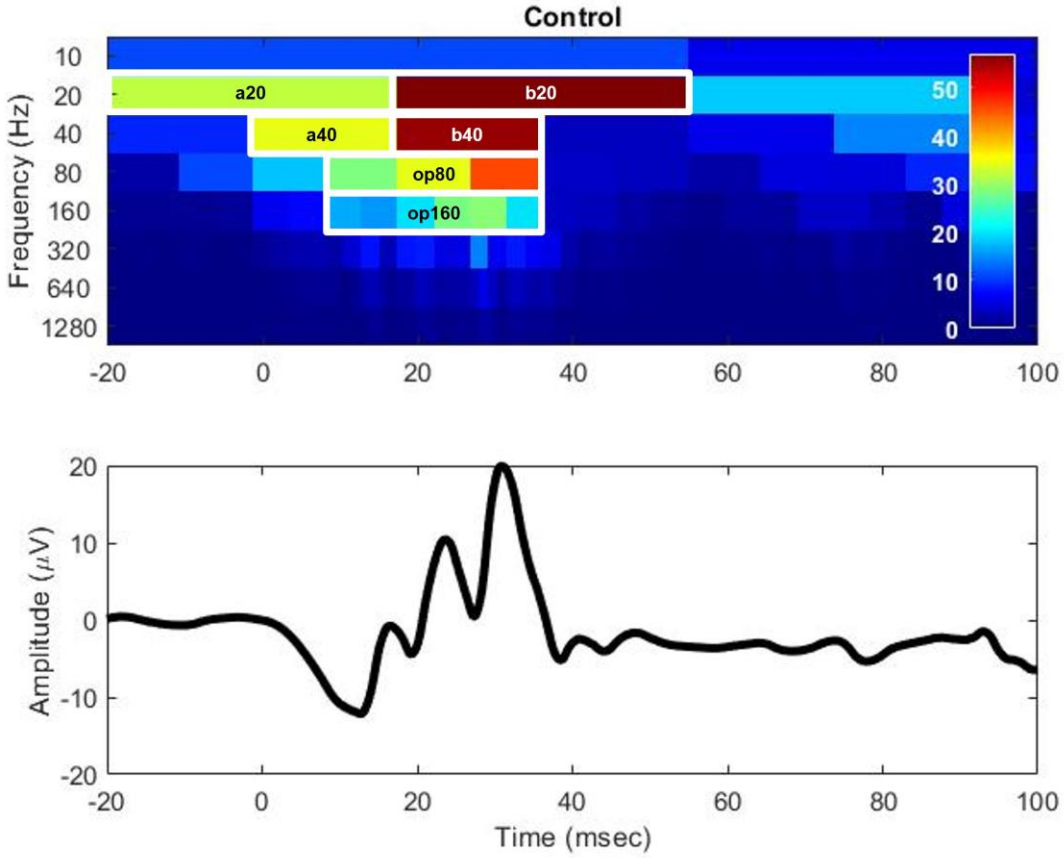

Figure 3: Time-Frequency spectrum (TFS) of the ERG waveform signal. The DWT coefficients, a20, a40, b20, and b40 correspond to the a- and b-wave with the 20Hz corresponding to the ON-pathway and 40Hz to the OFF-pathway. The op80 and op160 components relate to the early and later oscillatory potentials (OPs) that occur on the ascending limb of the b-wave. The upper figure shows the time-frequency DWT and the lower figure the raw time domain electroretinogram waveform.

wave peaks of the ERG signal are contained within the low frequency region specifically within (0-40) Hz characterized by 20a, 40a, 20b, and 40b descriptors respectively [32]. The early and later OPs are contained in the higher frequency regions (80 and 160 Hz) characterized by 80 OPs and 160 OPs respectively [34].

In this study, we obtained additional statistical features to the time-domain parameters (T_a, T_b, V_a, and V_b) including the approximate entropy of the DWT coefficients and used those values to

train ML models for ASD detection (section 2.5). We explored two different wavelet families, named 'Haar' and 'Symlet' as they have been used previously to analyze ERG waveform signals [34], [35]. To compare the same central frequencies proposed by Gauvin et al. [32] we up-sampled the signal from 2,000 Hz to 2,560 Hz and then performed a six-level decomposition. To provide an equitable comparison of the performance of 'Haar' and 'Symlet' wavelets using the proposed central frequency by Gauvin et al. [34], we used the 'Sym 2' wavelet instead of 'Sym 5' because the maximum possible decomposition levels using 'Sym 5' is 4, whereas the maximum possible decomposition levels using 'Sym 2' is 6 for the ERG waveform signal.

3.3.3. Variable Frequency Complex Demodulation (VFCDM)

Although wavelet transform is most useful in cases that require good time and frequency resolution in the high and low frequency ranges respectively [79]. VFCDM provides an alternative TFS analysis strategy that provides the highest time-frequency resolution whilst simultaneously preserving the accurate amplitude distribution of the original signal [79]. VFCDM has previously been used extensively to analyze different physiological signals [80], [81], [37] but to date it has not been applied to the ERG waveform signal.

The VFCDM method is described mathematically as follows:

Let a modulating signal x(t) whose frequency varies with time shown in equation (2) where A(t), $\theta(t)$, and dc(t) refers to the instantaneous amplitude, phase, and direct current component, respectively.

$$x(t) = dc(t) + A(t)(cos \int_0^t [2\pi f(\tau)d\tau + \theta(t)]) \quad (2)$$

We can extract the instantaneous amplitude, A(t), and phase by multiplying the original signal x(t) with $e^{-j\int_0^t 2\pi f(\tau)dt}$ as shown in equation (3) which causes a left shift in the spectrum of y(t).

$$\begin{aligned} y(t) &= x(t)e^{-j\int_0^t 2\pi f(\tau)dt} \\ &= dc(t)e^{-j\int_0^t 2\pi f(\tau)dt} + \frac{A(t)}{2}\, e^{j\theta(t)} + \frac{A(t)}{2} e^{-j\int_0^t 4\pi f(\tau)dt} \end{aligned} \quad (3)$$

Filtering y(t) with an appropriate ideal low pass filter (LPF) whose cutoff frequency f_c is lower than the central frequency f_o yields the components of interest $y_{LP}(t)$ with the same instantaneous amplitude A(t) and phase $\theta(t)$ as shown in equations (4), (5) and (6).

$$y_{LP}(t) = \frac{A(t)}{2}\, e^{j\theta(t)} \quad (4)$$

$$A(t) = 2|y_{LP}(t) \quad (5)$$

$$\theta(t) = tan^{-1}\{\frac{img(y_{LP}(t))}{real(y_{LP}(t))}\} \quad (6)$$

The instantaneous frequency can be estimated by equation (7) as reported in [82] where f_o is the center frequency of the varying frequency bands.

$$f(t) = f_o + \frac{1}{2\pi}\frac{d\theta(t)}{dt} \quad (7)$$

By using this complex demodulation and appropriate LPF technique, the original signal x(t) can be decomposed into sinusoid modulations (components) $d_i(t)$ as shown in equation (8). The instantaneous amplitude and frequency of components can then be determined by the Hilbert transform.

$$x(t) = d_i(t) \ = dc(t) + \sum_i A_i(t)(cos \int_0^t [2\pi f_i(\tau)d\tau + \theta_i(t)]) \quad (8)$$

We applied this TFS analysis technique to analyze the ERG waveform signals. First, the ERG waveform signal was decomposed into 24 components or frequency bands using VFCDM, so that each component contained a spectrum of approximately 41.67 Hz. Since the ERG signal was band-pass filtered to the range of 0.4 to 300 Hz, and the original sampling frequency was 2000 Hz, we considered only the first 8 VFCDM components, as they contained the most relevant information. Figure 4 shows the first 8 VFCDM components and their respective power spectral density. We removed the last 25 sample points from each of the VFCDM components to discard border effects. We calculated several statistical features from the first 8 VFCDM components to perform ML.

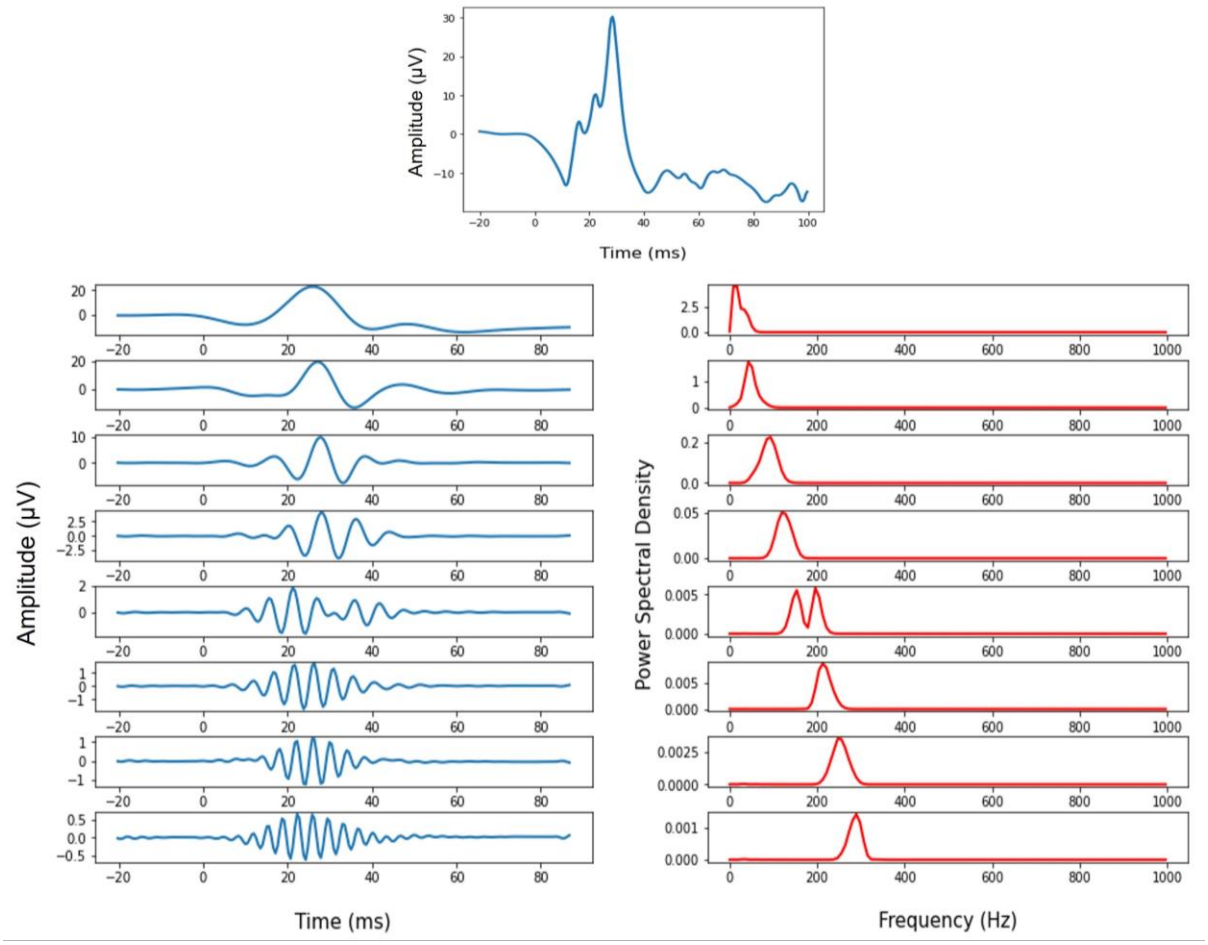

Figure 4: First 8 VFCDM components of the original ERG signal and their respective power spectral density.

Table 1: Feature set for DWT based ML models

Category	Features
Time-domain	T_a, V_a, T_b, V_b, ApEn of the ERG signal
Discrete Wavelet Transform	Mean, Median, Variance, Standard Variation, 25th percentile, 75th percentile, Inter-Quartile range (IQR), Kurtosis, Skewness

Table 2: Feature set for VFCDM based ML models

Category	Features
Time-domain	T_a, V_a, T_b, V_b
VFCDM decomposition	Maximum, Variance, IQR, ApEn, IQR, Kurtosis, Skewness

Tables 1 & 2 summarize the different features computed from the DWT and the VFCDM components. The time-domain indices were (T_a, V_a, T_b, V_b) used for both wavelet and VFCDM based ML models. For DWT-based ML models the approximate entropy (ApEn) [83],[84] of the original ERG signal was calculated because DWT performs downsampling which leaves less data points after the 4/5th decomposition to compute entropy. However, for VFCDM-based ML models, we computed the ApEn of VFCDM components instead of the original ERG signal. The entropy of a signal represents the unpredictability of fluctuations over time. Since ASD affects the oscillatory potentials of the ERG signal, which are seen as high frequency oscillations on the ascending limb of the b-wave, we intended to capture the changes in the randomness of the different frequency bands within the ERG signal.

3.4. Statistical analysis

We conducted a statistical comparison between the control and ASD groups for each of the time-domain, DWT, and VFCDM features listed in table 2, for the different combinations of the two flash strengths and eyes. Both time-domain indices and TFS features did not follow a normal distribution based on the Shapiro-Wilk normality test [85] and thus we tested if these indices differed significantly using a non-parametric T-test (Mann Whitney-U test). To provide a bottom line control vs ASD classification performance, for each time-domain index that exhibited a statistically significant difference between groups we used receiver operating characteristic analysis and defined the optimum threshold based on the maximum Youden's index (J) [86]. Youden's J index is defined as the difference between true positive rate (TPR) and the false positive rate (FPR) [86].

3.5. Machine Learning Classification

Using the extracted time-domain, DWT, and VFCDM features, we applied different ML algorithms to classify ASD from the comparison control group. We tested the following ML techniques: RF, AdaBoost, GradBoost, XGBoost, KNN, hyperplane-based discriminative classifier SVM, and MLP classifiers. The dataset comprised the full field light adapted ERG waveform signals from the 217 participants. Sometimes we had more than one sample (repeated measurements were used to replicate and validate the response) from a given subject for the same flash strength and eye. To ensure that the samples (replicates) from the same subject were not present in both the training and testing set, we applied a 10-fold subject-wise cross-validation. We divided the whole dataset into 10 subsets of subjects and used 9 of those subsets as a training set while the remaining subsets were used as the testing sets (maintaining the fact that any replicates were either in the training or testing set). We then repeated this 10 times. Note that we used the ERG signals from the right and left eyes that were acquired with two flash strengths (113 Td.s and 446 Td.s) in each subject. We trained separate ML models with data from each combination of eye/flash strength, to determine the best combination for detecting the ASD group.

As listed in Tables 1 & 2, we computed 54 features for DWT (n=54) and 56 features for VFCDM (n=56) based ML models, decompositions of which some may not have carried useful information. Some of these features may carry redundant and repetitive information which needed to be removed. To eliminate the extraneous features, we used a mean decrease in the impurity-based approach using RF to select the most informative features [87]. This method computed the average impurity decrease from each feature while training the RF, which then provided a feature importance percentage. We calculated the mean feature importance across all features and selected only those with a feature importance greater than 75% of the mean importance. This feature selection procedure decreased the overall model complexity and training time, along with improving the overall performance. We then performed 'GridsearchCV' [88] a popular exhaustive hyperparameter optimization strategy to find the optimal parameters for each of these classifiers. We used a subject-independent group 3-fold cross-validation strategy on the training data to avoid subject bias in the parameter optimization process. The best set of hyperparameters was then selected based on the highest average cross-validation F1-score. We used this F1-score as the scoring metric while optimizing hyperparameters because the F1-score is a better metric in cases of imbalanced datasets when regular accuracy can be misleading [89].

Another consideration in ML was the balance of the classes. In this study, for each combination of flash strength and eye the dataset was not balanced which could create a bias towards the majority class. Therefore, we tested several oversampling techniques such as the synthetic minority oversampling technique (SMOTE) [90], adaptive synthesis [91], and borderline SMOTE [92] to create synthetic samples of the minority class which enabled us to improve the sensitivity and specificity. The highest classification performance was achieved using borderline

SMOTE. Since borderline SMOTE only performs oversampling of the minority class without undersampling the majority class, the ASD group had the same number of samples as the control group after performing oversampling. As mentioned earlier we followed a subject-independent validation strategy to ensure the classification performance was more generalizable. We selected three easily interpretable performance criteria i.e., AUC-score, sensitivity, and specificity to evaluate the ML models. These metrics are defined as:

$$Sensitivity = \frac{TP}{TP+FN} \tag{9}$$

$$Specificity = \frac{TN}{FP+TN} \tag{10}$$

$$AUC\ score = Area\ under\ the\ ROC\ curve \tag{11}$$

where TP represents true positives, FP is total False Negatives, TN is the total number of true negatives and FN is the total false negatives.

The AUC score describes how good the model was at distinguishing between the control and ASD groups with the higher the AUC score the better the model and gives an overall measure of the ML performance. For biomedical applications, the model performance must be good for both positive (ASD) and negative (control) classes. Sensitivity and specificity provide further information on how good the model is at detecting the positive and negative classes, respectively. To further evaluate the models we computed the robust coefficient of variation (RCOV) of the AUC score defined as the ratio of median absolute deviation and median [93]. For consistently performing ML modes RCOV score should be small since the RCOV score tells the variability with respect to the median

4. Results

We found no significant differences between groups for iris color in the right or left eye ($p>.29$, Mann-Whitney U test). There were no significant group differences for the height of the right or left electrode ($p>.19$, Mann-Whitney U test). This is important because the amplitude of the recorded ERG signal will vary with electrode position [94] and iris color [78].. Table 3 summarizes the total number of samples for each combination of strength and eye. Note that we have multiple samples of repeated measures within the participants for each flash strength and eye combination.

Table 3: Total ERG samples for different combinations of Flash strength and eye

Flash Strength (Td.s)	Eye	Control	ASD
446	Right	310	183
	Left	325	172
113	Right	313	182

	Left	318	159

4.1. Classification using Time-Domain Analysis

Figure 5 shows the distribution of the time-domain indices along with their statistical comparisons between the control and ASD groups. The highest AUC scores of 0.67 and 0.66 were achieved using V_a or V_b as the predictors in the case of the 446 Td.s flash strength for the right eye. For full details see Table 1s in the supplementary information on thresholding on time-domain parameters.

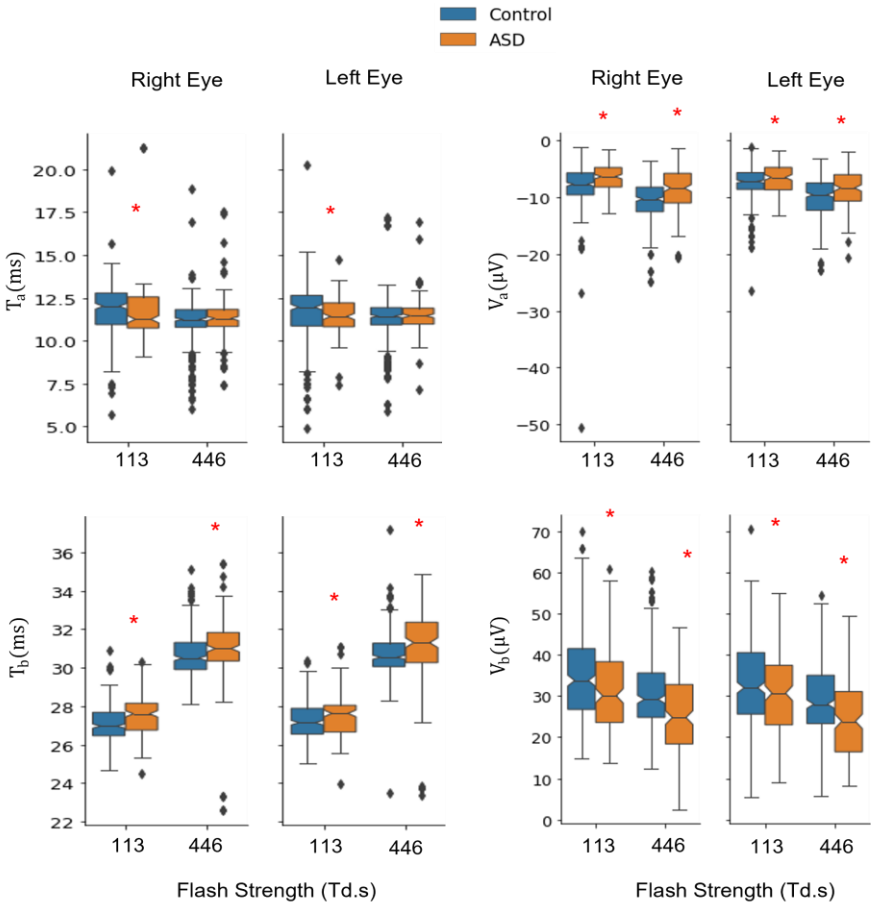

Figure 5: Statistical comparison between time-domain indices based on Mann Whitney-U test for each eye at each flash strength. Red asterisk (*) refers to statistically significant ($p<.05$) difference to the comparison group.

4.2. Machine Learning Classification using Spectral Analysis

In this subsection, we report the classification performance of the ML models discussed in the previous section for each combination of strength and eye. First, we discuss the results of

the DWT-based approach and compare the classification performance using the 'Sym 2' wavelet against the 'Haar' wavelet which has been used previously to analyze the ERG waveform signals [33], [35]. We then compared these DWT-based approaches to the results obtained using features from the VFCDM components. Finally, we discuss the best ERG recording configuration across the three abovementioned approaches. Figure 6 shows the bar plots of the AUC scores using 'Haar', 'Sym 2', and 'VFCDM' based features, respectively.

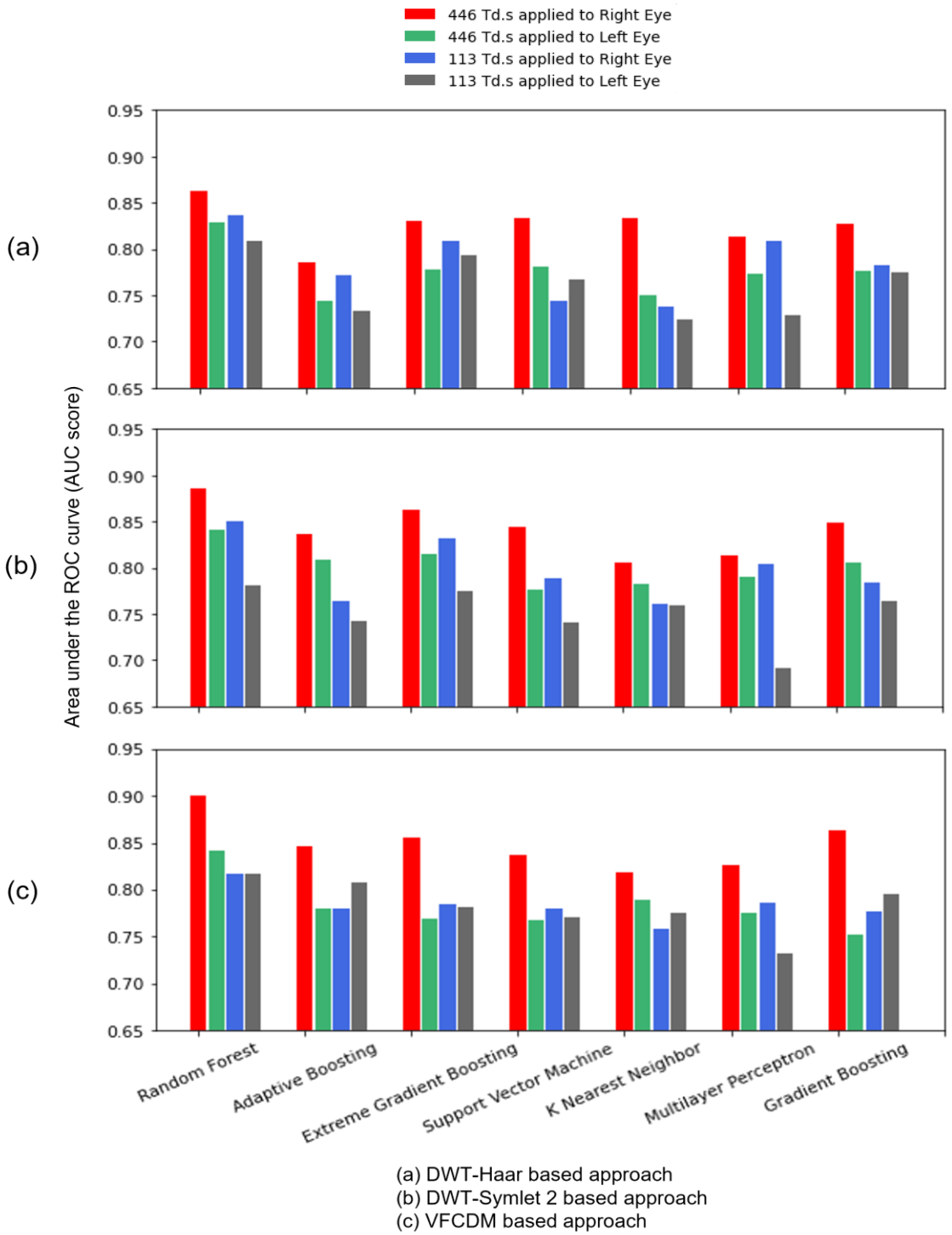

Figure 6: Classification overall performance (AUC score) using different spectral decomposition techniques. The RE 446 Td.s using RF provided the strongest AUC performance.

Figure 6 shows that for time-domain, DWT, and VFCDM features, the 446 Td.s/right eye combination achieved the best classification performance. As for the ML model comparison, the RF provided the highest classification performance compared to other classifiers. For this specific combination of strength and eye (446 Td.s/right eye) using 'Haar' wavelet-based features, we were able to classify ASD individuals with an 0.86 AUC score whereas using 'Sym 2' wavelet features provided a slightly higher AUC score of 0.88. Note the similar performance across all the classifiers. 'Sym 2' features provide either similar or better classification performance compared to 'Haar'. However, higher classification performance was achieved using features computed from the VFCDM component analysis. The RF model was able to detect ASD individuals with an AUC score of 0.90 for the same case of 446 Td.s applied to the right eye. To further compare these spectral analysis techniques, we provide the specificity and sensitivity in table 4 which shows the overall classification performance of the ML models using different spectral decomposition methods with VFCDM right eye at 446 Td.s providing the highest sensitivity of 0.85 and specificity of 0.78 with an AUC score of 0.90.

Table 4: Classification result using machine learning models (With Borderline SMOTE)

Spectral Analysis Technique	Classifier	Flash strength (Td.s)	Eye	Sensitivity	Specificity	AUC-Score
DWT-Haar	Random Forest	446	Right	0.74	0.79	0.86
DWT-Symlet 2				0.78	0.78	0.88
VFCDM				**0.85**	**0.78**	**0.90**
Haar	AdaBoost	446	Right	0.73	0.73	0.78
Symlet 2				0.84	0.72	0.84
VFCDM				0.88	0.69	0.85
Haar	XGBoost	446	Right	0.71	0.82	0.83
Symlet 2				0.79	0.76	0.86
VFCDM				0.82	0.76	0.86
Haar	SVM	446	Right	0.70	0.83	0.83
Symlet 2				0.81	0.75	0.84
VFCDM				0.76	0.80	0.84
Haar	KNN	446	Right	0.74	0.75	0.83
Symlet 2				0.78	0.67	0.80
VFCDM				0.84	0.65	0.82
Haar	MLP	446	Right	0.72	0.80	0.81
Symlet 2				0.75	0.76	0.81
VFCDM				0.77	0.78	0.83

Haar	GradBoost	446	Right	0.72	0.77	0.83
Symlet 2				0.82	0.76	0.84
VFCDM				0.83	0.78	0.86

To further validate the application of borderline SMOTE we also report classification results achieved without balancing the dataset. As shown in Table 3, the majority of the samples were from the control class, ML models were therefore biased toward the majority class. Classification results for 446/Right Eye and VFCDM-based decomposition are reported in Table 2 of the Supplementary Material, since this combination allowed the best separation between the control and ASD individuals.

Since we performed a 10-fold cross-validation on the whole dataset, we assessed how these classifiers performed for each fold along with the overall performance to ensure that the classifier was performing adequately for the whole dataset, which is an indication of the generalizability of the model. Figure 7 shows the boxplots along with 95% confidence intervals (around the median) and RCOV of AUC scores for the three different spectral analysis techniques with the 446 Td.s/Right Eye combination.

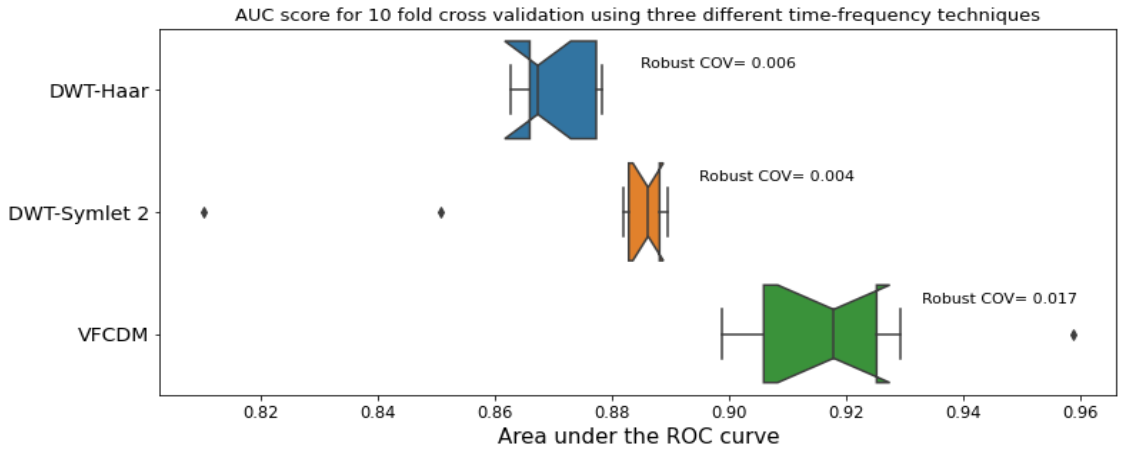

Figure 7: Boxplots of AUC scores (with 95% CI) for different spectral analysis techniques for the 446 Td.s/Right Eye combination.

The box plots appear flipped because the confidence interval exceeded the quartile values. The most important information conveyed by figure 7 is that the VFCDM spectral analysis technique allowed the ML to better classify ASD individuals from controls. Note that even though the VFCDM-based approach has the highest RCOV, the RCOV value is still small enough to support model generalizability. Both the 95% confidence interval and RCOV score show that the model is performing similarly for different parts of the data (different folds). In the next section, we will discuss which feature from the ERG waveform signal was the most important and contributed the most to the best overall group classification.

4.3. Feature Importance Analysis

First, we used an impurity reduction-based feature selection technique using the RF classifier which provided the feature importance but did not give any indication of how these features were impacting the overall model output. For this reason, we used an ML model explaining technique, named Shapley Additive Explanations (SHAP), to assess the feature contributions to the final output along with their overall respective feature importance [95]. To see how the classifier performed on the entire dataset (446 Td.s/Right eye) we split the dataset into training (80%) and testing (20%) sets maintaining the fact that all samples from the same subject were included in either the training or the test set. Using VFCDM features, the RF classifier achieved an AUC score of 0.92 with 0.87 sensitivity and 0.83 specificity on the test dataset which again corroborates the model generalizability.

We used the SHAP summary plots to visualize the effects of the 15 most important features (calculated from VFCDM components) in Figure 8, where the topmost features are the strongest for classification of the groups. Feature importance as assessed by the SHAP value agreed with the feature importance provided by RF. From Figure 8 the IQR of the 6^{th}, 7^{th}, and 8^{th} VFCDM components were the three most important features, as they had the highest SHAP value. In addition, the ASD participants tended to have a longer b-wave peak time (T_b) which is consistent with previous findings at this flash strength [25] as shown in Figure 5 lower left panel. However, figure 8 is especially important in showing that features from the higher frequency

range components were the most important ones in classifying the two groups with the five most important features contained within the 80 Hz to 300 Hz bands.

4.4. Failure Case Study

In the previous section, we discussed SHAP-based feature analysis where we divided the dataset (446 Td.s/Right Eye) into two groups where 80% of the data was in the training set and

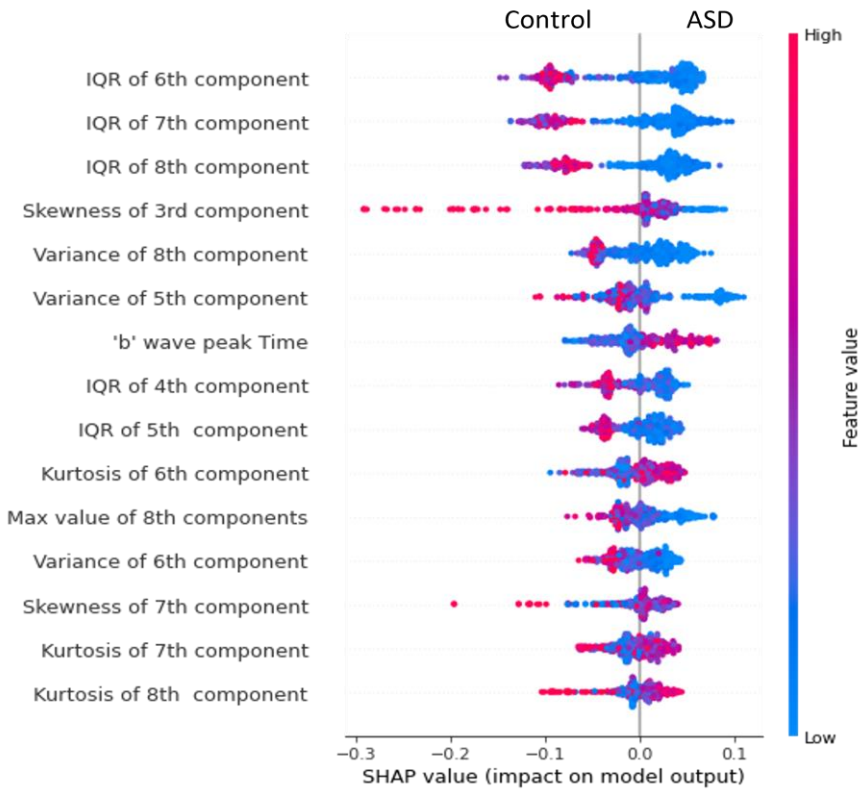

Figure 8: Feature importance of VFCDM ML model based on SHAP value.

the remaining 20% data were used as the test set. We had 85 samples in the testing dataset and out of that 71 samples were classified correctly, and 14 samples were classified incorrectly. To analyze why our proposed model was incorrectly classifying those 14 samples from the testing dataset, we performed statistical testing on time-domain and TFS features. Figure 9 shows how the time-domain and TFS features were distributed between control and ASD groups for both correctly and incorrectly classified samples.

Note that the correctly classified ASD samples have higher b-wave time to peak and a reduced b-wave amplitude peak voltage compared to the incorrectly classified control samples. This is in agreement with previous studies' reports on ASD subjects [25]. For the incorrectly classified samples, ASD and Control time-domain features' values overlapped, as ASD samples

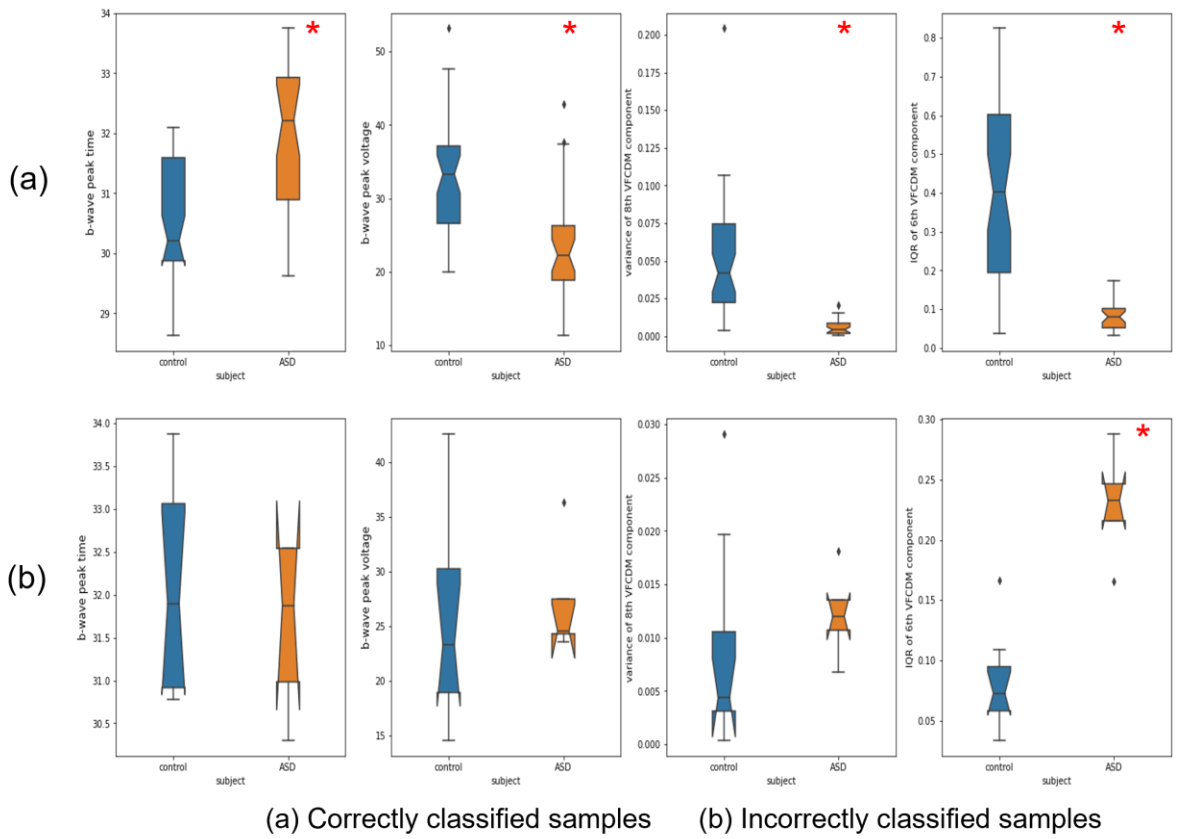

Figure 9: Distribution of TD and TFS features for correctly and incorrectly classified samples. Red asterisk (*) refers to statistically significant ($p<.05$) different.

showed particularly high b-wave time to peak and low b-wave peak amplitude voltage, with an opposite trend for the incorrectly classified control samples. In the case of TFS features, the distribution of features followed opposite trends between correctly and incorrectly classified ASD and control samples. The separation between control and ASD groups using both time-domain and TFS features for incorrectly classified samples was weak and followed an opposite trend compared to the correctly classified samples.

5. Discussion

We found that the VFCDM decomposition of the ERG waveform provided the most sensitive features to categorize ASD from Control groups using a Random Forest ML algorithm to achieve an AUC score of (0.92), with a sensitivity (0.85), and specificity (0.78) which outperformed models using DWT or time-domain features. Furthermore, we found evidence that the higher frequency range (80 – 300 Hz) carried the most relevant information and that the 446 Td.s flash strength delivered to the right eye allowed for the best ASD detection. The results presented in this paper demonstrate the potential of TFS analysis of ERG signals in identifying the ASD phenotype. Our results further indicate that the performance of threshold classification using

time-domain features was low when using one flash strength, with a maximum AUC score of 0.67 supporting the potential of TFS analysis to improve ASD classification in this population from the control group .

We built ML models using the features computed from DWT and VFCDM TFS analysis techniques. We followed the same ML analysis pipeline for each of the techniques. We compared the classification performance for 'Haar' and 'Sym 2' mother wavelets and found that 'Sym 2' was better at classifying ASD individuals. We used another very high-resolution spectral decomposition technique named VFCDM and showed that VFCDM achieves superior classification performance compared to wavelet-based analysis of ERG signal which has been previously proposed as a potential method for classifying ASD [36].

Previous studies have reported AUC score of approximately 0.70 using time-domain indices whereas using VFCDM-based features we have improved the AUC Score to 0.92 [68]. Previous studies based on eye movement reported ASD detection with approximately 85% accuracy but eye movement can be affected by several external factors [96]. A higher ASD detection performance with 95% positive predictive value (PPV) for certain age groups was reported using EEG signals but this technique required specialist skills and the data collection procedure was cumbersome [12]. A recent study has reported 99.5% accuracy using geographical information of the subjects and responses to standard questionnaires [97]. However, this approach did not provide an objective assessment of neurodevelopmental disorders. Whole cortex magnetoencephalography [98] and natural language processing based approaches [99] have been explored in previous studies to detect ASD subjects with relatively lower classification performance. HRV indices such as standard deviation of Normal to Normal interval and coefficient of variance were found to be significantly different between the control and ASD groups [9]. These previous approaches reported promising results but certain drawbacks such as complex procedures and the effect of external factors made these methods difficult to establish a biomarker and a tool to detect ASD quickly and accurately in a clinical setting. In contrast, retinal responses assessed by the ERG is a relatively easy and short procedure, less affected by external conditions which makes it suitable for establishing a potential biomarker to classify ASD. The ERG is used as a screening tool for diabetes [100] and glaucoma [101] as examples of its clinical utility. Table 6 summarizes and compares previously reported literature with our proposed method.

Table 6: Previously reported studies and our proposed method to detect ASD

Study	Method	Accuracy	Sensitivity	Specificity	AUC-score
Constable et al. [68]	Statistical analysis on b-wave peak time	NA	0.70	0.65	0.74
Wan et al. [96]	Eye tracking	0.85	0.86	0.83	NA

Bosl et al. [12]	Statistical measures of EEG features	NA	1.0	0.99	PPV=0.95
Raj et al. [97]	Geographical information of the subjects	0.99	0.98	0.96	NA
Roberts et al. [98]	Delayed auditory evoked response	NA	0.75	0.81	PPV=0.86
Elbattah et al. [99]	Eye tracking	NA	NA	NA	0.84
Kang et al. [55]	EEG and eye tracking	0.85	NA	NA	0.93
Carette et al. [54]	Eye tracking	0.83	NA	NA	0.90
Proposed method	**VFCDM analysis of the electroretinogram**	**0.81**	**0.85**	**0.78**	**0.90**

Our results on the analysis of the most important features are consistent with previous studies. For example, Gauvin et al. [102] reported that OPs contained in the high frequency range are usually affected in vasculopathy such as diabetic retinopathy [103], whereas the a-wave and b-wave (contained in the low frequency range) remain comparatively intact. For ASD, which is a neurodevelopmental disorder, we found similar results because features from the high frequency regions contained the most useful information for detecting ASD, indicating that TFS analysis effectively extracted the OPs, and they were sensitive for the detection of ASD. Figure 10 shows the strength of separation between control and ASD groups for different time-domain indices and TFS features for all data in the right and left eyes. Importantly, the light adapted OPs have been identified previously as being atypical in ASD in shape and energy [33], [64].

TFS features provided better separation compared to time-domain indices and the highest significant difference between the control and ASD group was found using VFCDM features with the lowest p-value. Moreover, figure 10 shows that features with the highest separation between the Control and ASD groups were from the higher frequency range (both wavelet and VFCDM) which is consistent with findings from the SHAP summary plot. Taken

together, these results indicate that ASD mostly affects the OPs of the ERG signal that derives from the amacrine cells and suggests a deficit in the dopaminergic signaling pathway [104], [105].

In this study, we have also provided additional evidence about the optimal ERG data collection configuration for ASD detection (light strength and eye). In our analysis, two flash

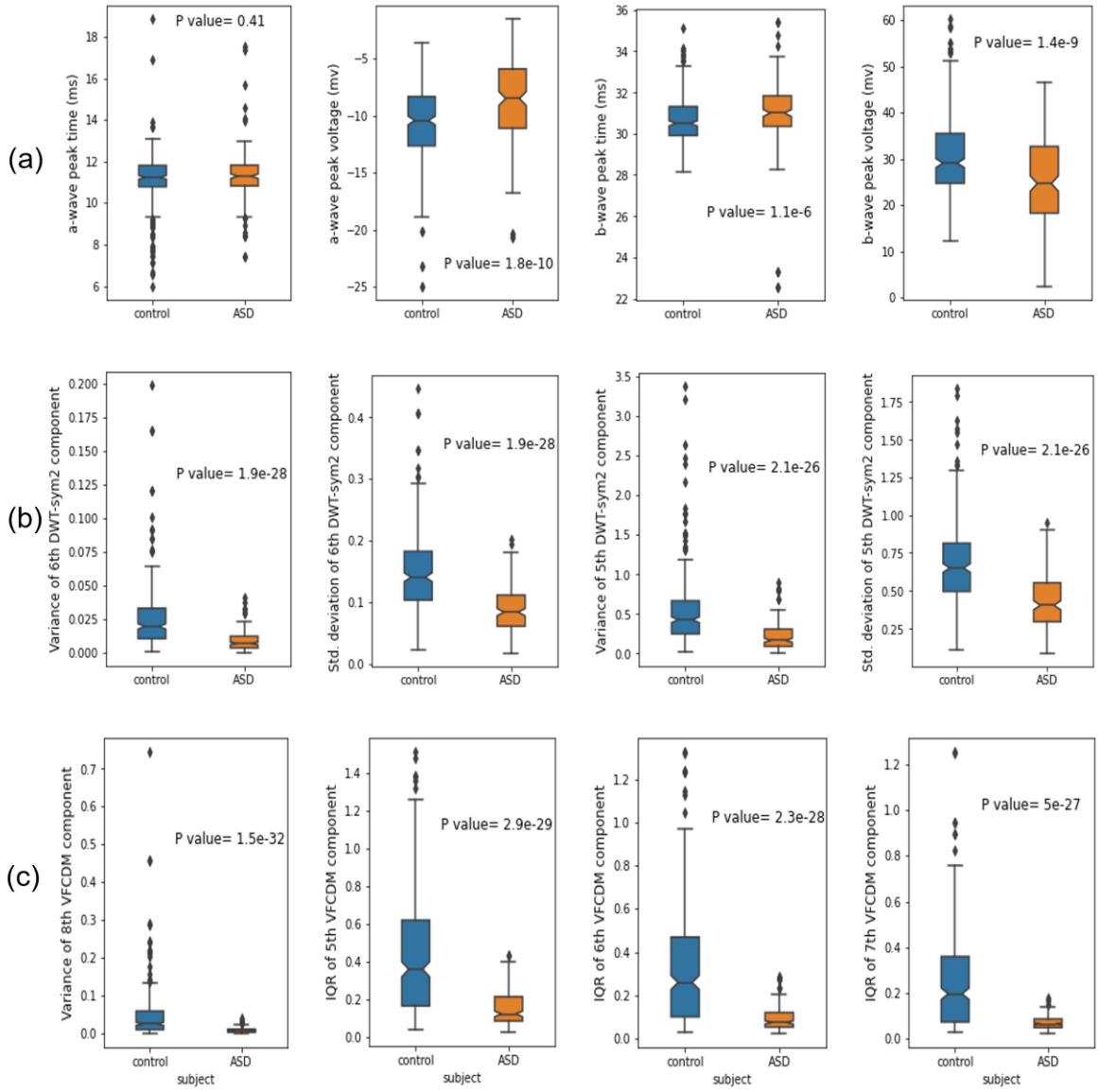

(a) Time domain indices
(b) First 4 DWT-Symlet 2 features with highest significant difference
(c) First 4 VFCDM features with highest significant difference

Figure 10: Time-domain indices and time-frequency features (446/Right eye) with highest separation between control and ASD groups based on non-parametric T-test (Mann

strengths were evaluated for signal processing techniques based on previous studies that have identified a significant group differences at these flash strengths which correspond to the

photopic hill peak dominated by the OFF- pathway within the retina and the plateau phase of the photopic hill dominated by the ON-pathway of the retina [68], [31], [106]. We found that the 446 Td.s flash strength provided comparatively better classification performance than the 113 Td.s flash strength. We also found that classification performance was better for signals collected from the right eye which we speculate may be due to the right eye's data being collected first and the participants may have been more alert with better fixation. Another factor may be that we found that the RETeval was easier to handle using the right hand rather than the left hand for the left eye and thus the responses for the left eye tended to be lower in our hands. There is no physiological reason why one eye may be lower in amplitude than the other and the firmware version (2.12.0) at the time precluded randomization of eye or beginning a test session with the left eye first to balance for testing order.

One limitation is that in this study we restricted the populations to those with a sole diagnosis of ASD and we cannot at this stage determine if the strength of the classification will hold in cases where individuals meet more than one diagnostic classification such as ADHD and ASD which can co-occur [107]. Furthermore, the effects of gender, prior medication use, and developmental or chronological age may need to be further investigated to determine any effects on the validity of any classification model. Nevertheless, we demonstrate the possibility of using the ERG as a tool in identifying the ASD phenotype through spectral-domain analysis that may complement further biomarker studies in this field [108].

6. Conclusion

We have demonstrated the feasibility of the TFS analysis using VFCDM for extracting information from ERG waveform signals for the detection of ASD. Using VFCDM features, machine learning models achieved an AUC score of 0.92, sensitivity of 0.85, and specificity of 0.78, outperforming DWT and time-domain features. Finally, the best ASD detection was achieved when ERG was obtained using a flash strength of 446 Td.s applied to the right eye. As for future directions of our work, we are planning to expand our dataset for further improvement of our methods. More ERG samples from ASD and control subjects will allow us to increase the generalizability of the proposed machine learning models. With a larger dataset, we could also try combining features from both eyes without overfitting the models. If the dataset is large enough (an international collaboration, for example), we will also be able to use deep learning (neural networks with more than three layers) to detect ASD from raw ERG signals or TFS of ERG. Furthermore, incorporating other signals such as the heart rate variability, EDA, and pupillary light response as part of a multimodal approach could help improve the ASD detection performance of ML models. Future studies could also explore the suitability of ERG in diagnosing other related neurodevelopmental disorders such as ADHD.

References

[1] “Park HR, Lee JM, Moon HE, et al. A Short Review on the Current Understanding of Autism Spectrum Disorders. Exp Neurobiol. 2016;25(1):1-13. doi:10.5607/en.2016.25.1.1”.

[2] “Lord C, Elsabbagh M, Baird G, Veenstra-Vanderweele J. Autism spectrum disorder. Lancet. 2018 Aug 11;392(10146):508-520. doi: 10.1016/S0140-6736(18)31129-2. Epub 2018 Aug 2. PMID: 30078460; PMCID: PMC7398158.”.

[3] “Hyman SL, Levy SE, Myers SM; COUNCIL ON CHILDREN WITH DISABILITIES, SECTION ON DEVELOPMENTAL AND BEHAVIORAL PEDIATRICS. Identification, Evaluation, and Management of Children With Autism Spectrum Disorder. Pediatrics. 2020 Jan;145(1):e20193447. doi: 10.1542/peds.2019-3447. Epub 2019 Dec 16. PMID: 31843864.”.

[4] “McCarty P, Frye RE. Early Detection and Diagnosis of Autism Spectrum Disorder: Why Is It So Difficult? Semin Pediatr Neurol. 2020 Oct;35:100831. doi: 10.1016/j.spen.2020.100831. Epub 2020 Jun 24. PMID: 32892958.”.

[5] “Wen, T.H., Cheng, A., Andreason, C. et al. Large scale validation of an early-age eye-tracking biomarker of an autism spectrum disorder subtype. Sci Rep 12, 4253 (2022). https://doi.org/10.1038/s41598-022-08102-6”.

[6] “Shic, F., Naples, A.J., Barney, E.C. et al. The Autism Biomarkers Consortium for Clinical Trials: evaluation of a battery of candidate eye-tracking biomarkers for use in autism clinical trials. Molecular Autism 13, 15 (2022). https://doi.org/10.1186/s13229-021-00482-2”.

[7] “Klin A. Biomarkers in Autism Spectrum Disorder: Challenges, Advances, and the Need for Biomarkers of Relevance to Public Health. Focus (Am Psychiatr Publ). 2018 Apr;16(2):135-142. doi: 10.1176/appi.focus.20170047. Epub 2018 Apr 27. PMID: 31975908; PMCID: PMC6526849.”.

[8] “Schmitt, L.M., Cook, E.H., Sweeney, J.A. et al. Saccadic eye movement abnormalities in autism spectrum disorder indicate dysfunctions in cerebellum and brainstem. Molecular Autism 5, 47 (2014). https://doi.org/10.1186/2040-2392-5-47”.

[9] “Billeci L, Tonacci A, Narzisi A, Manigrasso Z, Varanini M, Fulceri F, Lattarulo C, Calderoni S, Muratori F. Heart Rate Variability During a Joint Attention Task in Toddlers With Autism Spectrum Disorders. Front Physiol. 2018 May 1;9:467. doi: 10.3389/fphys.2018.00467. PMID: 29765335; PMCID: PMC5938714.”.

[10] “Ferguson BJ, Hamlin T, Lantz JF, Villavicencio T, Coles J, Beversdorf DQ. Examining the Association Between Electrodermal Activity and Problem Behavior in Severe Autism Spectrum Disorder: A Feasibility Study. Front Psychiatry. 2019 Sep 11;10:654. doi: 10.3389/fpsyt.2019.00654. PMID: 31572238; PMCID: PMC6749070.”.

[11] “Bosl, W., Tierney, A., Tager-Flusberg, H. et al. EEG complexity as a biomarker for autism spectrum disorder risk. BMC Med 9, 18 (2011). https://doi.org/10.1186/1741-7015-9-18”.

[12] “Bosl, W.J., Tager-Flusberg, H. & Nelson, C.A. EEG Analytics for Early Detection of Autism Spectrum Disorder: A data-driven approach. Sci Rep 8, 6828 (2018). https://doi.org/10.1038/s41598-018-24318-x”.

[13] “Puce, A., & Hämäläinen, M. S. (2017). A Review of Issues Related to Data Acquisition and Analysis in EEG/MEG Studies. Brain sciences, 7(6), 58. https://doi.org/10.3390/brainsci7060058”.

[14] “M. -B. Hossain, H. F. Posada-Quintero and K. H. Chon, ‘A Deep Convolutional Autoencoder for Automatic Motion Artifact Removal in Electrodermal Activity,’ in IEEE Transactions on Biomedical Engineering, vol. 69, no. 12, pp. 3601-3611, Dec. 2022, doi: 10.1109/TBME.2022.3174509.”.

[15] "Kim HG, Cheon EJ, Bai DS, Lee YH, Koo BH. Stress and Heart Rate Variability: A Meta-Analysis and Review of the Literature. Psychiatry Investig. 2018 Mar;15(3):235-245. doi: 10.30773/pi.2017.08.17. Epub 2018 Feb 28. PMID: 29486547; PMCID: PMC5900369.".
[16] "London A, Benhar I, Schwartz M. The retina as a window to the brain-from eye research to CNS disorders. Nat Rev Neurol. 2013 Jan;9(1):44-53. doi: 10.1038/nrneurol.2012.227. Epub 2012 Nov 20. PMID: 23165340.".
[17] "Almonte MT, Capellàn P, Yap TE, Cordeiro MF. Retinal correlates of psychiatric disorders. Ther Adv Chronic Dis. 2020 Mar 9;11:2040622320905215. doi: 10.1177/2040622320905215. PMID: 32215197; PMCID: PMC7065291.".
[18] "Schwitzer T, Le Cam S, Cosker E, Vinsard H, Leguay A, Angioi-Duprez K, Laprevote V, Ranta R, Schwan R, Dorr VL. Retinal electroretinogram features can detect depression state and treatment response in adults: A machine learning approach. J Affect Disord. 2022 Jun 1;306:208-214. doi: 10.1016/j.jad.2022.03.025. Epub 2022 Mar 15. PMID: 35301040.".
[19] "Silverstein SM, Thompson JL. Progress, Possibilities, and Pitfalls in Electroretinography Research in Psychiatry. Biol Psychiatry. 2020 Feb 1;87(3):202-203. doi: 10.1016/j.biopsych.2019.10.028. PMID: 31908288.".
[20] "Yang, X.L. (2004). Characterization of receptors for glutamate and GABA in retinal neurons. Prog Neurobiol 73(2), 127-150. doi: 10.1016/j.pneurobio.2004.04.002.".
[21] "Zhou, Y., and Danbolt, N.C. (2013). GABA and Glutamate Transporters in Brain. Front Endocrinol (Lausanne) 4, 165. doi: 10.3389/fendo.2013.00165.".
[22] "Lavoie J, Illiano P, Sotnikova TD, Gainetdinov RR, Beaulieu JM, Hébert M. The electroretinogram as a biomarker of central dopamine and serotonin: potential relevance to psychiatric disorders. Biol Psychiatry. 2014 Mar 15;75(6):479-86. doi: 10.1016/j.biopsych.2012.11.024. Epub 2013 Jan 7. PMID: 23305992.".
[23] "Naaijen, J., Bralten, J., Poelmans, G., consortium, I., Glennon, J.C., Franke, B., et al. (2017). Glutamatergic and GABAergic gene sets in attention-deficit/hyperactivity disorder: association to overlapping traits in ADHD and autism. Transl Psychiatry 7(1), e999. doi: 10.1038/tp.2016.273.".
[24] "Constable PA, Lim JKH, Thompson DA. Retinal electrophysiology in central nervous system disorders. A review of human and mouse studies. Front Neurosci. 2023 Aug 2;17:1215097. doi: 10.3389/fnins.2023.1215097. PMID: 37600004; PMCID: PMC10433210.".
[25] "Lee, I. O., D. H. Skuse, P. A. Constable, F. Marmolejo-Ramos, L. R. Olsen and D. A. Thompson (2022). 'The electroretinogram b-wave amplitude: a differential physiological measure for Attention Deficit Hyperactivity Disorder and Autism Spectrum Disorder.' J Neurodev Disord 14(1): 30.".
[26] "Constable PA, Gaigg SB, Bowler DM, Jägle H, Thompson DA. Full-field electroretinogram in autism spectrum disorder. Doc Ophthalmol. 2016 Apr;132(2):83-99. doi: 10.1007/s10633-016-9529-y. Epub 2016 Feb 11. PMID: 26868825.".
[27] "Ritvo ER, Creel D, Realmuto G, Crandall AS, Freeman BJ, Bateman JB, Barr R, Pingree C, Coleman M, Purple R. Electroretinograms in autism: a pilot study of b-wave amplitudes. Am J Psychiatry. 1988 Feb;145(2):229-32. doi: 10.1176/ajp.145.2.229. PMID: 3341467.".
[28] "Friedel EBN, Schäfer M, Endres D, Maier S, Runge K, Bach M, Heinrich SP, Ebert D, Domschke K, Tebartz van Elst L, Nickel K. Electroretinography in adults with high-functioning autism spectrum disorder. Autism Res. 2022 Nov;15(11):2026-2037. doi: 10.1002/aur.2823. Epub 2022 Oct 10. PMID: 36217563.".
[29] "Hébert M, Mérette C, Gagné AM, Paccalet T, Moreau I, Lavoie J, Maziade M. The Electroretinogram May Differentiate Schizophrenia From Bipolar Disorder. Biol Psychiatry. 2020 Feb 1;87(3):263-270. doi: 10.1016/j.biopsych.2019.06.014. Epub 2019 Jun 27. PMID: 31443935.".
[30] "Demmin DL, Davis Q, Roché M, Silverstein SM. Electroretinographic anomalies in schizophrenia. J Abnorm Psychol. 2018 May;127(4):417-428. doi: 10.1037/abn0000347. PMID: 29745706.".

[31] "Hamilton R, Bees MA, Chaplin CA, McCulloch DL. The luminance-response function of the human photopic electroretinogram: a mathematical model. Vision Res. 2007 Oct;47(23):2968-72. doi: 10.1016/j.visres.2007.04.020. Epub 2007 Sep 24. PMID: 17889925.".
[32] "Gauvin M, Lina JM, Lachapelle P. Advance in ERG analysis: from peak time and amplitude to frequency, power, and energy. Biomed Res Int. 2014;2014:246096. doi: 10.1155/2014/246096. Epub 2014 Jul 1. PMID: 25061605; PMCID: PMC4100345.".
[33] "Constable PA, Marmolejo-Ramos F, Gauthier M, Lee IO, Skuse DH, Thompson DA. Discrete Wavelet Transform Analysis of the Electroretinogram in Autism Spectrum Disorder and Attention Deficit Hyperactivity Disorder. Front Neurosci. 2022 Jun 6;16:890461. doi: 10.3389/fnins.2022.890461. PMID: 35733935; PMCID: PMC9207322.".
[34] "Gauvin M, Sustar M, Little JM, Brecelj J, Lina JM, Lachapelle P. Quantifying the ON and OFF Contributions to the Flash ERG with the Discrete Wavelet Transform. Transl Vis Sci Technol. 2017 Jan 10;6(1):3. doi: 10.1167/tvst.6.1.3. PMID: 28097047; PMCID: PMC5235331.".
[35] "Gauvin M, Little JM, Lina JM, Lachapelle P. Functional decomposition of the human ERG based on the discrete wavelet transform. J Vis. 2015;15(16):14. doi: 10.1167/15.16.14. PMID: 26746684.".
[36] "S. M. Manjur et al., 'Detecting Autism Spectrum Disorder Using Spectral Analysis of Electroretinogram and Machine Learning: Preliminary results,' 2022 44th Annual International Conference of the IEEE Engineering in Medicine & Biology Society (EMBC), 2022, pp. 3435-3438, doi: 10.1109/EMBC48229.2022.9871173.".
[37] "Bashar SK, Walkey AJ, McManus DD, Chon KH. VERB: VFCDM-Based Electrocardiogram Reconstruction and Beat Detection Algorithm. IEEE Access. 2019;7:13856-13866. doi: 10.1109/ACCESS.2019.2894092. Epub 2019 Jan 21. PMID: 31741809; PMCID: PMC6860377.".
[38] "Hossain MB, Bashar SK, Lazaro J, Reljin N, Noh Y, Chon KH. A robust ECG denoising technique using variable frequency complex demodulation. Comput Methods Programs Biomed. 2021 Mar;200:105856. doi: 10.1016/j.cmpb.2020.105856. Epub 2020 Nov 21. PMID: 33309076; PMCID: PMC7920915.".
[39] "Aşuroğlu, T., Oğul, H. A deep learning approach for parkinson's disease severity assessment. Health Technol. 12, 943–953 (2022). https://doi.org/10.1007/s12553-022-00698-z".
[40] "Jerome H. Friedman. 'Greedy function approximation: A gradient boosting machine..' Ann. Statist. 29 (5) 1189 - 1232, October 2001. https://doi.org/10.1214/aos/1013203451".
[41] "Schapire, R. E. (2013). Explaining adaboost. In Empirical inference (pp. 37–52). Springer.".
[42] "Chen, T., & Guestrin, C. (2016). XGBoost: A Scalable Tree Boosting System. In Proceedings of the 22nd ACM SIGKDD International Conference on Knowledge Discovery and Data Mining (pp. 785–794). New York, NY, USA: ACM. https://doi.org/10.1145/2939672.2939785".
[43] "Cortes, C., & Vapnik, V. (1995). Support-vector networks. Machine Learning, 20(3), 273–297.".
[44] "Mucherino, A., Papajorgji, P.J., Pardalos, P.M. (2009). k-Nearest Neighbor Classification. In: Data Mining in Agriculture. Springer Optimization and Its Applications, vol 34. Springer, New York, NY. https://doi.org/10.1007/978-0-387-88615-2_4".
[45] "Haykin, S. (1994). Neural networks: a comprehensive foundation. Prentice Hall PTR.".
[46] "Lord, C., Risi, S., Lambrecht, L. et al. The Autism Diagnostic Observation Schedule—Generic: A Standard Measure of Social and Communication Deficits Associated with the Spectrum of Autism. J Autism Dev Disord 30, 205–223 (2000). https://doi.org/10.1023/A:1005592401947".
[47] "Lord C, Rutter M, Le Couteur A. Autism Diagnostic Interview-Revised: a revised version of a diagnostic interview for caregivers of individuals with possible pervasive developmental disorders. J Autism Dev Disord. 1994 Oct;24(5):659-85. doi: 10.1007/BF02172145. PMID: 7814313.".
[48] "Minissi, M.E., Chicchi Giglioli, I.A., Mantovani, F. et al. Assessment of the Autism Spectrum Disorder Based on Machine Learning and Social Visual Attention: A Systematic Review. J Autism Dev Disord 52, 2187–2202 (2022). https://doi.org/10.1007/s10803-021-05106-5".

[49] “Schopler E, Reichler RJ, DeVellis RF, Daly K. Toward objective classification of childhood autism: Childhood Autism Rating Scale (CARS). J Autism Dev Disord. 1980 Mar;10(1):91-103. doi: 10.1007/BF02408436. PMID: 6927682.”.
[50] “Rutter, M., Bailey, A. and Lord, C. (2003) The Social Communication Questionnaire: Manual. Western Psychological Services, Los Angeles.”.
[51] “Constantino, J.N. (2013). Social Responsiveness Scale. In: Volkmar, F.R. (eds) Encyclopedia of Autism Spectrum Disorders. Springer, New York, NY. https://doi.org/10.1007/978-1-4419-1698-3_296”.
[52] “Skuse D, Warrington R, Bishop D, Chowdhury U, Lau J, Mandy W, Place M. The developmental, dimensional and diagnostic interview (3di): a novel computerized assessment for autism spectrum disorders. J Am Acad Child Adolesc Psychiatry. 2004 May;43(5):548-58. doi: 10.1097/00004583-200405000-00008. PMID: 15100561.”.
[53] “Hus Y, Segal O. Challenges Surrounding the Diagnosis of Autism in Children. Neuropsychiatr Dis Treat. 2021 Dec 3;17:3509-3529. doi: 10.2147/NDT.S282569. PMID: 34898983; PMCID: PMC8654688.”.
[54] “Carette, Romuald & Elbattah, Mahmoud & Cilia, Federica & Dequen, Gilles & Guerin, Jean-Luc & Bosche, Jérôme. (2019). Learning to Predict Autism Spectrum Disorder based on the Visual Patterns of Eye-tracking Scanpaths. 103-112. 10.5220/0007402601030112.”.
[55] “Kang J, Han X, Song J, Niu Z, Li X. The identification of children with autism spectrum disorder by SVM approach on EEG and eye-tracking data. Comput Biol Med. 2020 May;120:103722. doi: 10.1016/j.compbiomed.2020.103722. Epub 2020 Mar 23. PMID: 32250854.”.
[56] “Matlis S, Boric K, Chu CJ, Kramer MA. Robust disruptions in electroencephalogram cortical oscillations and large-scale functional networks in autism. BMC Neurol. 2015 Jun 27;15:97. doi: 10.1186/s12883-015-0355-8. Erratum in: BMC Neurol. 2015;15:142. PMID: 26111798; PMCID: PMC4482270.”.
[57] “Ismail MM, Keynton RS, Mostapha MM, ElTanboly AH, Casanova MF, Gimel’farb GL, El-Baz A. Studying Autism Spectrum Disorder with Structural and Diffusion Magnetic Resonance Imaging: A Survey. Front Hum Neurosci. 2016 May 11;10:211. doi: 10.3389/fnhum.2016.00211. PMID: 27242476; PMCID: PMC4862981.”.
[58] “Shoeibi, A., Sadeghi, D., Moridian, P., Ghassemi, N., Heras, J., Alizadehsani, R., Khadem, A., Kong, Y., Nahavandi, S., Zhang, Y., & Górriz, J.M. (2021). Automatic Diagnosis of Schizophrenia in EEG Signals Using CNN-LSTM Models. Frontiers in Neuroinformatics, 15.”.
[59] “Ari B, Sobahi N, Alçin ÖF, Sengur A, Acharya UR. Accurate detection of autism using Douglas-Peucker algorithm, sparse coding based feature mapping and convolutional neural network techniques with EEG signals. Comput Biol Med. 2022 Feb 9;143:105311. doi: 10.1016/j.compbiomed.2022.105311. Epub ahead of print. PMID: 35158117.”.
[60] “Posada-Quintero HF, Chon KH. Innovations in Electrodermal Activity Data Collection and Signal Processing: A Systematic Review. Sensors (Basel). 2020 Jan 15;20(2):479. doi: 10.3390/s20020479. PMID: 31952141; PMCID: PMC7014446.”.
[61] “Ghiasi, S., Greco, A., Barbieri, R. et al. Assessing Autonomic Function from Electrodermal Activity and Heart Rate Variability During Cold-Pressor Test and Emotional Challenge. Sci Rep 10, 5406 (2020). https://doi.org/10.1038/s41598-020-62225-2”.
[62] “Prince EB, Kim ES, Wall CA, Gisin E, Goodwin MS, Simmons ES, Chawarska K, Shic F. The relationship between autism symptoms and arousal level in toddlers with autism spectrum disorder, as measured by electrodermal activity. Autism. 2017 May;21(4):504-508. doi: 10.1177/1362361316648816. Epub 2016 Jun 10. PMID: 27289132; PMCID: PMC5812779.”.

[63] “Panju, S., Brian, J., Dupuis, A. et al. Atypical sympathetic arousal in children with autism spectrum disorder and its association with anxiety symptomatology. Molecular Autism 6, 64 (2015). https://doi.org/10.1186/s13229-015-0057-5”.
[64] “Constable, P.A., Gaigg, S.B., Bowler, D.M. et al. Full-field electroretinogram in autism spectrum disorder. Doc Ophthalmol 132, 83–99 (2016). https://doi.org/10.1007/s10633-016-9529-y”.
[65] “Constable PA, Ritvo ER, Ritvo AR, Lee IO, McNair ML, Stahl D, Sowden J, Quinn S, Skuse DH, Thompson DA, McPartland JC. Light-Adapted Electroretinogram Differences in Autism Spectrum Disorder. J Autism Dev Disord. 2020 Aug;50(8):2874-2885. doi: 10.1007/s10803-020-04396-5. PMID: 32034650.”.
[66] “Constable PA, Lee IO, Marmolejo-Ramos F, Skuse DH, Thompson DA. The photopic negative response in autism spectrum disorder. Clin Exp Optom. 2021 Nov;104(8):841-847. doi: 10.1080/08164622.2021.1903808. Epub 2021 Apr 7. PMID: 33826873.”.
[67] “Youssef, P., Nath, S., Chaimowitz, G., & Prat, S. (2019). Electroretinography in psychiatry: A systematic literature review. European Psychiatry, 62, 97-106. doi:10.1016/j.eurpsy.2019.09.006”.
[68] “Constable, P.A., Ritvo, E.R., Ritvo, A.R. et al. Light-Adapted Electroretinogram Differences in Autism Spectrum Disorder. J Autism Dev Disord 50, 2874–2885 (2020). https://doi.org/10.1007/s10803-020-04396-5”.
[69] “Constable PA, Lee IO, Marmolejo-Ramos F, Skuse DH, Thompson DA. The photopic negative response in autism spectrum disorder. Clin Exp Optom. 2021 Nov;104(8):841-847. doi: 10.1080/08164622.2021.1903808. Epub 2021 Apr 7. PMID: 33826873.”.
[70] “Neveu MM, Dangour A, Allen E, Robson AG, Bird AC, Uauy R, Holder GE. Electroretinogram measures in a septuagenarian population. Doc Ophthalmol. 2011 Oct;123(2):75-81. doi: 10.1007/s10633-011-9282-1. Epub 2011 Aug 4. PMID: 21814827.”.
[71] “APA, Diagnostic and statistical manual of mental disorders (DSM-IV-TR). 2000, Washington DC, USA: American Psychiatric Association.”.
[72] “APA, Diagnostic and Statistical Manual of Mental Disorders V, ed. R. Adamczyk. 2013, Arlington VA: American Psychiatric Association.”.
[73] “Lord C, Rutter M, Goode S, Heemsbergen J, Jordan H, Mawhood L, Schopler E. Autism diagnostic observation schedule: a standardized observation of communicative and social behavior. J Autism Dev Disord. 1989 Jun;19(2):185-212. doi: 10.1007/BF02211841. PMID: 2745388.”.
[74] “Gotham K, Risi S, Pickles A, Lord C. The Autism Diagnostic Observation Schedule: revised algorithms for improved diagnostic validity. J Autism Dev Disord. 2007 Apr;37(4):613-27. doi: 10.1007/s10803-006-0280-1. Epub 2006 Dec 16. PMID: 17180459.”.
[75] “Robson AG, Frishman LJ, Grigg J, Hamilton R, Jeffrey BG, Kondo M, Li S, McCulloch DL. ISCEV Standard for full-field clinical electroretinography (2022 update). Doc Ophthalmol. 2022 Jun;144(3):165-177. doi: 10.1007/s10633-022-09872-0. Epub 2022 May 5. PMID: 35511377; PMCID: PMC9192408.”.
[76] “Al Abdlseaed A, McTaggart Y, Ramage T, Hamilton R, McCulloch DL. Light- and dark-adapted electroretinograms (ERGs) and ocular pigmentation: comparison of brown- and blue-eyed cohorts. Doc Ophthalmol. 2010 Oct;121(2):135-46. doi: 10.1007/s10633-010-9240-3. Epub 2010 Jul 28. PMID: 20665068.”.
[77] “Asi H, Perlman I. Relationships between the electroretinogram a-wave, b-wave and oscillatory potentials and their application to clinical diagnosis. Doc Ophthalmol. 1992;79(2):125-39. doi: 10.1007/BF00156572. PMID: 1591967.”.
[78] “Thompson DA, Feather S, Stanescu HC, Freudenthal B, Zdebik AA, Warth R, Ognjanovic M, Hulton SA, Wassmer E, van’t Hoff W, Russell-Eggitt I, Dobbie A, Sheridan E, Kleta R, Bockenhauer D. Altered electroretinograms in patients with KCNJ10 mutations and EAST syndrome. J Physiol. 2011 Apr

1;589(Pt 7):1681-9. doi: 10.1113/jphysiol.2010.198531. Epub 2011 Feb 7. PMID: 21300747; PMCID: PMC3099023.".
[79] "Wang H, Siu K, Ju K, Chon KH. A high resolution approach to estimating time-frequency spectra and their amplitudes. Ann Biomed Eng. 2006 Feb;34(2):326-38. doi: 10.1007/s10439-005-9035-y. Epub 2006 Feb 7. PMID: 16463086.".
[80] "Posada-Quintero HF, Chon KH. Innovations in Electrodermal Activity Data Collection and Signal Processing: A Systematic Review. Sensors (Basel). 2020;20(2):479. Published 2020 Jan 15. doi:10.3390/s20020479".
[81] "Hossain MB, Bashar SK, Lazaro J, Reljin N, Noh Y, Chon KH. A robust ECG denoising technique using variable frequency complex demodulation. Comput Methods Programs Biomed. 2021 Mar;200:105856. doi: 10.1016/j.cmpb.2020.105856. Epub 2020 Nov 21. PMID: 33309076; PMCID: PMC7920915.".
[82] "Monti A, Médigue C, Mangin L. Instantaneous parameter estimation in cardiovascular time series by harmonic and time-frequency analysis. IEEE Trans Biomed Eng. 2002 Dec;49(12 Pt 2):1547-56. doi: 10.1109/TBME.2002.805478. PMID: 12549736.".
[83] "Pincus SM. Approximate entropy as a measure of system complexity. Proc Natl Acad Sci U S A. 1991 Mar 15;88(6):2297-301. doi: 10.1073/pnas.88.6.2297. PMID: 11607165; PMCID: PMC51218.".
[84] "Pincus SM, Gladstone IM, Ehrenkranz RA. A regularity statistic for medical data analysis. J Clin Monit. 1991 Oct;7(4):335-45. doi: 10.1007/BF01619355. PMID: 1744678.".
[85] "Marmolejo-Ramos, F., & González-Burgos, J. (2013). A power comparison of various tests of univariate normality on Ex-Gaussian distributions. Methodology: European Journal of Research Methods for the Behavioral and Social Sciences, 9(4), 137–149. https://doi.org/10.1027/1614-2241/a000059".
[86] "Schisterman, E. F., Perkins, N. J., Liu, A., & Bondell, H. (2005). Optimal Cut-Point and Its Corresponding Youden Index to Discriminate Individuals Using Pooled Blood Samples. Epidemiology, 16(1), 73–81. http://www.jstor.org/stable/20486002".
[87] "Speiser, J.L., Miller, M.I., Tooze, J.A., & Ip, E.H. (2019). A comparison of random forest variable selection methods for classification prediction modeling. Expert systems with applications, 134, 93-101 .".
[88] "LaValle SM, Branicky MS, Lindemann SR. On the Relationship between Classical Grid Search and Probabilistic Roadmaps. The International Journal of Robotics Research. 2004;23(7-8):673-692. doi:10.1177/0278364904045481".
[89] Z. Lipton, C. Elkan, and B. Narayanaswamy, "Thresholding Classifiers to Maximize F1 Score," Jan. 2014.
[90] "Nitesh V. Chawla, Kevin W. Bowyer, Lawrence O. Hall, and W. Philip Kegelmeyer. 2002. SMOTE: synthetic minority over-sampling technique. J. Artif. Int. Res. 16, 1 (January 2002), 321–357.".
[91] "Haibo He, Yang Bai, E. A. Garcia and Shutao Li, 'ADASYN: Adaptive synthetic sampling approach for imbalanced learning,' 2008 IEEE International Joint Conference on Neural Networks (IEEE World Congress on Computational Intelligence), 2008, pp. 1322-1328, doi: 10.1109/IJCNN.2008.4633969.".
[92] "Hien M. Nguyen, Eric W. Cooper, and Katsuari Kamei. 2011. Borderline over-sampling for imbalanced data classification. Int. J. Knowl. Eng. Soft Data Paradigm. 3, 1 (April 2011), 4–21. https://doi.org/10.1504/IJKESDP.2011.039875".
[93] R. Ospina and F. Marmolejo-Ramos, "Performance of Some Estimators of Relative Variability," *Frontiers in Applied Mathematics and Statistics*, vol. 5, Aug. 2019, doi: 10.3389/fams.2019.00043.
[94] "Hobby AE, Kozareva D, Yonova-Doing E, Hossain IT, Katta M, Huntjens B, Hammond CJ, Binns AM, Mahroo OA. Effect of varying skin surface electrode position on electroretinogram responses recorded using a handheld stimulating and recording system. Doc Ophthalmol. 2018 Oct;137(2):79-86. doi: 10.1007/s10633-018-9652-z. Epub 2018 Jul 25. PMID: 30046929; PMCID: PMC6153519.".

[95] “Scott M. Lundberg and Su-In Lee. 2017. A unified approach to interpreting model predictions. In Proceedings of the 31st International Conference on Neural Information Processing Systems (NIPS’17). Curran Associates Inc., Red Hook, NY, USA, 4768–4777.”.
[96] “Wan G, Kong X, Sun B, Yu S, Tu Y, Park J, Lang C, Koh M, Wei Z, Feng Z, Lin Y, Kong J. Applying Eye Tracking to Identify Autism Spectrum Disorder in Children. J Autism Dev Disord. 2019 Jan;49(1):209-215. doi: 10.1007/s10803-018-3690-y. PMID: 30097760.”.
[97] “Raj, Suman & Masood, Sarfaraz. (2020). Analysis and Detection of Autism Spectrum Disorder Using Machine Learning Techniques. Procedia Computer Science. 167. 994-1004. 10.1016/j.procs.2020.03.399.”.
[98] “Roberts TP, Khan SY, Rey M, Monroe JF, Cannon K, Blaskey L, Woldoff S, Qasmieh S, Gandal M, Schmidt GL, Zarnow DM, Levy SE, Edgar JC. MEG detection of delayed auditory evoked responses in autism spectrum disorders: towards an imaging biomarker for autism. Autism Res. 2010 Feb;3(1):8-18. doi: 10.1002/aur.111. PMID: 20063319; PMCID: PMC3099241.”.
[99] “M. Elbattah, J. -L. Guérin, R. Carette, F. Cilia and G. Dequen, ‘NLP-Based Approach to Detect Autism Spectrum Disorder in Saccadic Eye Movement,’ 2020 IEEE Symposium Series on Computational Intelligence (SSCI), 2020, pp. 1581-1587, doi: 10.1109/SSCI47803.2020.9308238.”.
[100] “Deng X, Li Z, Zeng P, Wang J, Liang J, Lan Y. A Diagnostic Model for Screening Diabetic Retinopathy Using the Hand-Held Electroretinogram Device RETeval. Front Endocrinol (Lausanne). 2021 Apr 12;12:632457. doi: 10.3389/fendo.2021.632457. PMID: 33912134; PMCID: PMC8074966.”.
[101] “Kita Y, Holló G, Saito T, Momota Y, Kita R, Tsunoda K, Hirakata A. RETeval Portable Electroretinogram Parameters in Different Severity Stages of Glaucoma. J Glaucoma. 2020 Jul;29(7):572-580. doi: 10.1097/IJG.0000000000001509. PMID: 32287150.”.
[102] “Gauvin M, Dorfman AL, Trang N, Gauthier M, Little JM, Lina JM, Lachapelle P. Assessing the Contribution of the Oscillatory Potentials to the Genesis of the Photopic ERG with the Discrete Wavelet Transform. Biomed Res Int. 2016;2016:2790194. doi: 10.1155/2016/2790194. Epub 2016 Dec 22. PMID: 28101507; PMCID: PMC5217158.”.
[103] “Midena E, Torresin T, Longhin E, Midena G, Pilotto E, Frizziero L. Early Microvascular and Oscillatory Potentials Changes in Human Diabetic Retina: Amacrine Cells and the Intraretinal Neurovascular Crosstalk. J Clin Med. 2021 Sep 7;10(18):4035. doi: 10.3390/jcm10184035. PMID: 34575150; PMCID: PMC8466765.”.
[104] “Wachtmeister L. Some aspects of the oscillatory response of the retina. Prog Brain Res. 2001;131:465-74. doi: 10.1016/s0079-6123(01)31037-3. PMID: 11420963.”.
[105] “Wachtmeister L. Oscillatory potentials in the retina: what do they reveal. Prog Retin Eye Res. 1998 Oct;17(4):485-521. doi: 10.1016/s1350-9462(98)00006-8. PMID: 9777648.”.
[106] “Johnson MA, Jeffrey BG, Messias AMV, Robson AG. ISCEV extended protocol for the stimulus-response series for the dark-adapted full-field ERG b-wave. Doc Ophthalmol. 2019 Jun;138(3):217-227. doi: 10.1007/s10633-019-09687-6. Epub 2019 Mar 30. PMID: 30929109.”.
[107] “Krakowski AD, Cost KT, Szatmari P, et al. Characterizing the ASD-ADHD phenotype: measurement structure and invariance in a clinical sample. Journal of Child Psychology and Psychiatry, and Allied Disciplines. 2022 Mar. DOI: 10.1111/jcpp.13609. PMID: 35342939.”.
[108] “Molloy CJ, Gallagher L. Can stratification biomarkers address the heterogeneity of autism spectrum disorder? Ir J Psychol Med. 2022 Sep;39(3):305-311. doi: 10.1017/ipm.2021.73. Epub 2021 Nov 26. PMID: 34823622.”.
[109] “de Vries L, Fouquaet I, Boets B, Naulaers G, Steyaert J. Autism spectrum disorder and pupillometry: A systematic review and meta-analysis. Neurosci Biobehav Rev. 2021 Jan;120:479-508. doi: 10.1016/j.neubiorev.2020.09.032. Epub 2020 Oct 22. PMID: 33172600.”.

[110] “Lynch G. Using Pupillometry to Assess the Atypical Pupillary Light Reflex and LC-NE System in ASD. Behav Sci (Basel). 2018 Nov 21;8(11):108. doi: 10.3390/bs8110108. PMID: 30469373; PMCID: PMC6262612.”.